Vol. 92 No. 1 pp. 56–73 ACTA GEOLOGICA SINICA (English Edition) Feb. 2018

Crustal Uplift in the Longmen Shan Mountains Revealed by Isostatic Gravity Anomalies along the Eastern Margin of the Tibetan Plateau

LI Yong[1], YAN Zhaokun[1,*], ZHOU Rongjun[2], YAN Liang[1], DONG Shunli[1], SHAO Chongjian[1] and LAURENCE Svirchev[1]

1 *State Key Laboratory of Oil and Gas Reservoir Geology and Exploitation, Chengdu University of Technology, Chengdu 610059, Sichuan, China*

2 *Institute of Earthquake Engineering, Seismological Bureau of Sichuan Province, 610041, Sichuan, China*

Abstract: This study examines the relationship between high positive isostatic gravity anomalies (IGA), steep topography and lower crustal extrusion at the eastern margin of the Tibetan Plateau. IGA data has revealed uplift and extrusion of lower crustal flow in the Longmen Shan Mountains (the LMS). Firstly, The high positive IGA zone corresponds to the LMS orogenic belt. It is shown that abrupt changes in IGA correspond to zones of abrupt change of topography, crustal thickness and rock density along the LMS. Secondly, on the basis of the Airy isostasy theory, simulations and inversions of the positive IGA were conducted using three-dimensional bodies. The results indicated that the LMS lacks a mountain root, and that the top surface of the lower crust has been elevated by 11 km, leading to positive IGA, tectonic load and density load. Thirdly, according to Watts's flexural isostasy model, elastic deflection occurs, suggesting that the limited (i.e. narrow) tectonic and density load driven by lower crustal flow in the LMS have led to asymmetric flexural subsidence in the foreland basin and lifting of the forebulge. Finally, based on the correspondence between zones of extremely high positive IGA and the presence of the Precambrian Pengguan-Baoxing complexes in the LMS, the first appearance of erosion gravels from the complexes in the Dayi Conglomerate layer of the Chengdu Basin suggest that positive IGA and lower crustal flow in the LMS took place at 3.6 Ma or slightly earlier.

Key words: isostatic gravity anomalies, crustal uplift, Longmen Shan Mountains, lower crustal flow, foreland basin, the eastern margin of the Tibetan Plateau

1 Introduction

The eastern margin of the Tibetan Plateau consists of three primary tectonic landforms units: the plateau (the eastern Tibetan Plateau), the mountains (the LMS orogenic belt), and the foreland basin (Chengdu Basin, or western Sichuan Basin), which are collectively known as the basin–mountain–plateau system (Li Yong et al., 2005). The LMS, which is located between the Tibetan Plateau and the Sichuan Basin, is a linear and asymmetrical marginal orogenic belt with an abrupt change in slope between the LMS and the front region (Densmore et al., 2005, 2007). Moreover, it is a complex geological body upon which several tectonic uplift mechanisms have been superimposed at various times since the Indosinian. Cenozoic tectonic deformations occurred mainly after 3.6 Ma (Li et al., 2006) and were superimposed on the Mesozoic orogenic belt (Burchfiel et al., 1995, 2008; Xu Zhiqin et al., 2007).

Following the 2008 Wenchuan Earthquake (Ms 8.0) and the 2013 Lushan Earthquake (Ms 7.0), studies of the LMS have attracted great attention to understand its uplifting, mass wasting and seismogenic mechanisms (Parker et al., 2011; Yan Zhaokun et al., 2016, 2017; Qiu Jun et al., 2017). To date, four types of uplift mechanisms have been proposed: crustal shortening (Hubbard and Shaw, 2009; Tan et al., 2016), extrusion (Xu Zhiqin et al., 2007), lower crustal flow (Royden et al., 1997; Clark and Royden, 2000; Simon et al., 2003; Enkelmann et al., 2006; Meng et al., 2006; Burchfiel et al., 2008; Kirby et al., 2008; Wang Qianshen et al., 2012; Li Yong et al., 2017), and crustal isostatic rebound (Densmore et al., 2005; Li et al., 2006; Fu et al., 2011; Molnar, 2012). Consequently, finding a

* Corresponding author. E-mail: yzk517@163.com

way to identify the uplift mechanisms of the LMS and major earthquakes remains a challenge. Since IGA is useful method of identifying lower crustal extrusion (Bird, 1991), elastic thickness (Burov and Diament, 1996) and uplift mechanisms in steep topography (Li Yong et al., 2005), our aim in this study was to examine the relationship between IGA and the steep topography, elastic thickness and lower crustal extrusion at the eastern margin of the Tibetan Plateau. Based on Airy's and Watts's isostasy models, we used a large-scale IGA framework to demonstrate that lower crustal flow is an important factor in the uplift of the LMS. The foreland basin is explicable, in outline, as flexure of the Yangtze Plate in response to tectonic loading related to lower crustal flow. An analytical simulation model was used to estimate the disturbance to the topography of the Mohorovicic discontinuity (Moho), tectonic loading, crustal structure, elastic thickness, flexure subsidence, uplift of the forebulge, the first appearance of positive IGA and lower crustal flow in the LMS.

2 Regional Tectonic Framework, Geophysical Field and Characters of Deep Structure

2.1 Regional tectonic framework

The eastern margin of Tibetan Plateau can be divided into two totally different tectonic units by the LMS tectonic belt. The eastern part is the stable Yangtze block, and the western part is the complex geological block combined with the Songpan-Garze fold belt. Moreover, the Yangtze block is a stable craton solidified during the Jinning period, and the sedimentation of typical platform covers on the late Proterozoic metamorphic basement. The strata is nearly horizontal and the deformation is weak. The Songpan-Garze fold belt is the product of the opening and closing of Paleo-Tethys Ocean. It experienced the process of shrink deformation, stretch deformation, and formed the deep high-temperature ductile shear zone, which accompanied with the tectonic deformation phenomenon of high-temperature foliation, lineation, A-model fold (Xu et al., 1992).

2.2 Regional Bouguer gravity anormaly characters and the thickness of crust

Bouguer gravitational field mainly reflects the tectonic and mass distribution in crust and upper-mantle. Fig. 1a shows the trend of the Bouguer gravity anormaly: all the Bouguer gravity anormaly values are negative (−70–−430mGal), and gradually decrease from east to west. Moreover, it is most noticeable that there is a Bouguer gravity gradient Zone, which grows at the direction of NNE, goes along the LMS. According to the form, the intensity, the isoline density and the spreading direction of Bouguer gravity anormaly, the study area can be divided into three parts (Fig. 1a). And through the inversion of Bouguer gravity anormaly, the thickness contours of crust

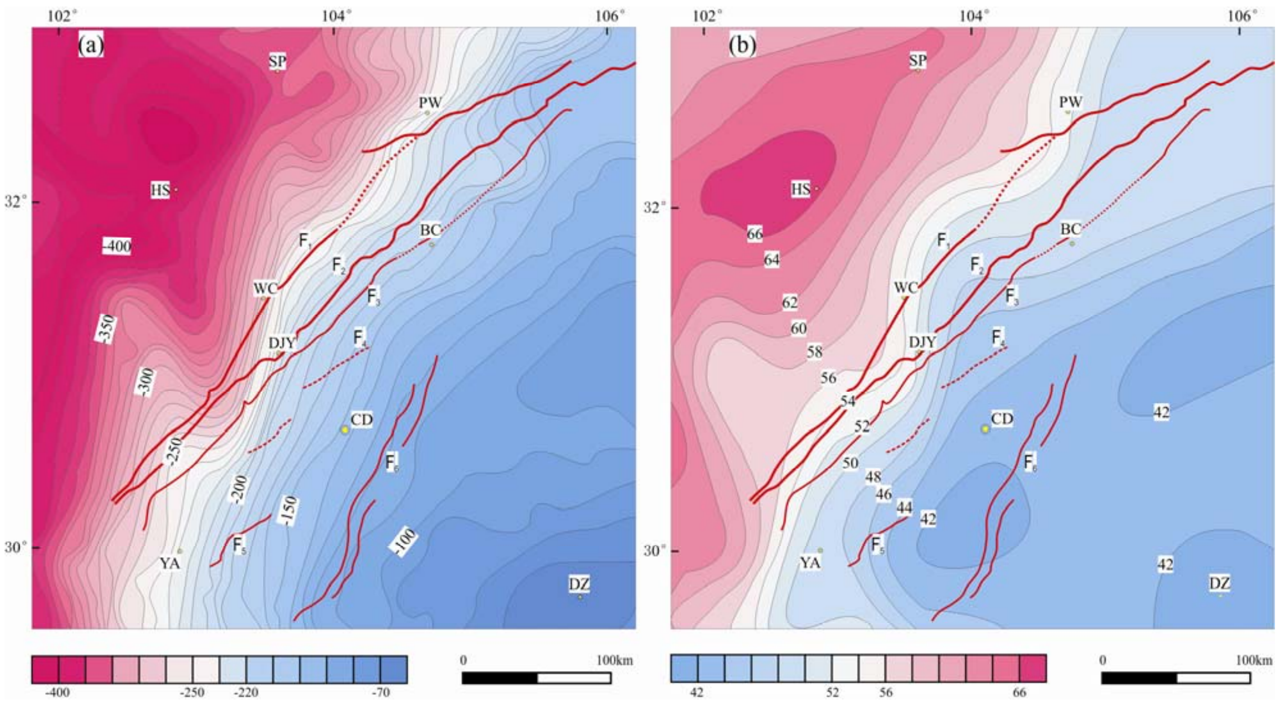

Fig. 1. The Bouguer gravity anomaly map (a) and the distribution of crustal thickness (b) of the eastern margin of Tibetan Plateau (modified from GPTSBGMR, 1991).

F_1=Maowen Fault; F_2=Beichuan Fault; F_3=Pengguan Fault; F_4=Dayi Fault; F_5=Xiongpo Fault; F_6=Longquan Shan Fault; CD=Chengdu; BC=Beichuan; DJY=Dujiangyan; WC=Wenchuan; PW=Pingwu; SP=Songpan; HS=Heishui; YA=Yaan; DZ=Dazu.

in this area can be obtained (fig. 1b). As Fig. 1b, the thickness of crust decrease from west to east, and the area also can be divided into three zones.

(1) Zone 1

Zone1 locates in the west of LMS. The Bouguer gravity anomaly values in Zone 1 are relative lower. The Bouguer gravity anomaly contours in this zone do not show the obvious dominant distribution direction. It means that the change of the crust thickness in this area is very small. The maximum thickness of crust in this area is 66km.

(2) Zone 2

Zone 2 locates in the LMS area. The Gravity anormaly values change abruptly in this zone, the average changing gradient is up to 2.2 mGal/km. So the Moho surface in this zone is a slope, which dips west. We can know that the crust thickness sharply increase from east to west in LMS area. The Moho steep dip to the west and the average gradient is up to 0.2 mGal /km. The LMS fault zone locates in the area with abrupt changes of Bouguer gravity anomaly and crust thickness, so the LMS fault zone is a deep fracture cutting to the upper mantle. We speculate that the Bouguer gravity anomaly high point is related to the Pengguan complex and the Baoxing complex.

(3) Zone 3

Zone 3 locates in the east of LMS. The Bouguer gravity anomaly values of this zone are relative higher. There is a closed Bouguer Gravity Anomaly relatively high-value area in Dazu city. The Bouguer gravity anomaly contour changes smoothly. It means that the change of the crust thickness in this zone is very small, and the minimum thickness crust of this area is in Dazu city, is about 42 km.

2.3 The deep tectonic structure characters

According to the geophysical profiles of Heishui-Chongqing-Xiushan, which across the eastern Tibetan Plateau (Fig. 2), we propose the following cognitions:

(1) In the study area, the lithospheric thickness changes abruptly from the Yangtze Block to the Songpan-Garze fold belt. The lithospheric thickness increases from 95km to 140km at the range of 80 km. This area locates in the LMS tectonic belt. It means that the LMS fault belt is a deep fracture cutting to the upper mantle. In this area, the large earthquakes (higher than 6 magnitude, especially higher than 7 magnitude) mainly occurred in this area (Fig. 2a).

(2) The depth of Moho surface is about 40km in the western margin of Yangtze Block, and there is an abnormal mantle under the Moho surface (Fig. 2b).

(3) There is a low velocity and low resistivity layer (the thickness is 3–5 km) under the lower crust (the depth is about 20 km) in the west of LMS. The low velocity and low resistivity layer maybe the detachment zone in the deep of the western Sichuan Plateau, and the depth this layer is consistent with the depth of most earthquakes in this area (Fig. 2c).

(4) The LMS tectonic belt is a wedge-shaped body shows thicker in the west part and thin in the east part. The upper part of the LMS tectonic belt is consisted by a series of rootless tectonic slices segmented by the imbricate thrust faults and listric thrust faults. It is a tectonic thrust wedge. The maximum thickness of the thrust wedge is 10km, and the maximum depth is 20 km. There is a horizontal slip layer under the thrust wedge, and there is a high resistivity and rigid block under the slip layer (Fig. 2d).

3 Research Objective

Isostatic gravity anomalies reflect the current isostatic state in a given region. They result from static and dynamic processes in the lithosphere and indicate the characteristics of recent tectonism and crustal structure. The Pratt and Airy isostatic models are two fundamental explanations of isostasy in a given region, in which isostatic compensation at a given site or region is considered to act in a vertical direction. Flexural isostasy models (Watts, 1992, 2001; Stewart and Watts, 1997; Jordan and Watts, 2005) propose horizontal isostatic compensation over a given region. The isostatic relationship between the orogenic belt and the foreland basin appear to be linked by flexural isostasy, which therefore becomes important in establishing the coupling mechanisms between the orogenic belt and the foreland basin. Several studies have conducted inversions of the positive IGA in the LMS using the Airy isostasy model (Li Yong et al., 2005; Wang Qianshen et al., 2008; Fu et al., 2014). In the present work, a flexural isostasy model based on IGA data at the eastern margin of the Tibetan Plateau revealed the crustal uplift mechanisms of the LMS and flexural subsidence in the foreland basin.

The objectives of this study were two-fold. Firstly, based on the Airy isostasy model, the relationship between the positive IGA and the lower crustal flow in the LMS was simulated to provide a rational explanation of the uplift mechanisms in these areas. Secondly, based on Watts's flexural isostasy model, the relationship between tectonic loading in the LMS and asymmetrical flexural subsidence in the foreland basin was simulated to investigate the dynamic coupling mechanisms between the basin and the mountains.

4 Research Method

Modern IGA values reflect the recent state of tectonic

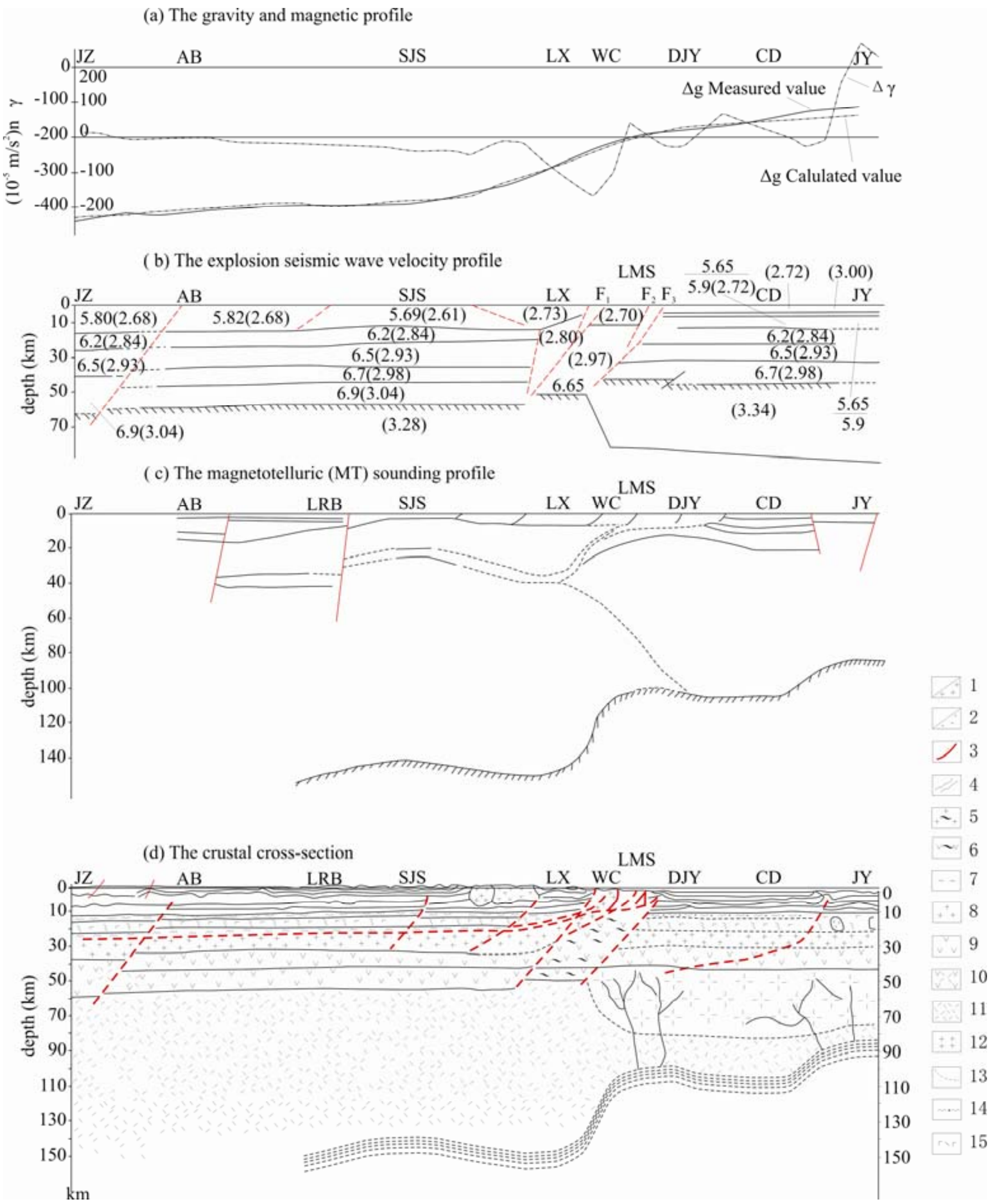

Fig. 2. The geophysical profile of the eastern margin of Tibetan Plateau (modified from GPTSBGMR, 1991).
F_1=Maowen Fault; F_2=Beichuan Fault; F_3=Pengguan Fault; JZ=Jiuzhi; AB=Aba; LRB=Longriba; SJS=Shuajingsi; LX=Lixian; DJY=Dujiangyan; CD=Chengdu; JY=Jianyang; 1=granite and quartz syenite from Mesoproterozoic to Jurassic; 2=quartz diorite from late Archaean to early Proterozoic; 3=thrust fault; 4=stratigraphic boundary of epimetamorphic rocks or sedimentary rock; 5=mixed granite rock; 6=collision complex; 7=plastic layer; 8=sial; 9=sima; 10=abnormal lower crust; 11=upper mantle; 12=anomalous upper mantle; 13=supposed fault; 14=Pre-sinian fold basement; 15=Pre-sinian crystalline basement.

activity in the deep crust. Because such activity tends to restore isostatic equilibrium, we plotted an IGA map of the eastern margin of the Tibetan Plateau and correlated it with tectonic landform units, topography and rock density in the region.

4.1 IGA map of the eastern margin of the Tibetan Plateau

Based on measured gravity data (1: 1,000,000) and in line with Airy's isostasy model (Fig. 3; Fig. 4) in this region, we performed global-scale corrections for height, mesosphere, topography and the normal field, as well as isostatic corrections. The raw gravity data comes from GPTSBGMR, who got the data with the accelerometer in 1988. The raw gravity data was kept by the GPTSBGMR, Chengdu, China. But the raw gravity data is kept confidential, so we can't provide the raw data. Based on the raw gravity data (the scale is 1: 1,000,000). We corrected the data with global altitude, middle layer, topography, normal field, and isostatic corrected according to Airy model. Then we plotted the isostatic gravity anomaly map of the eastern Tibetan Plateau (the scale is 1: 3,000,000, the precision of the isostatic gravity anomaly is 2×10^{-5} m/s^2, and contour interval is 5×10^{-5} m/s^2). The map

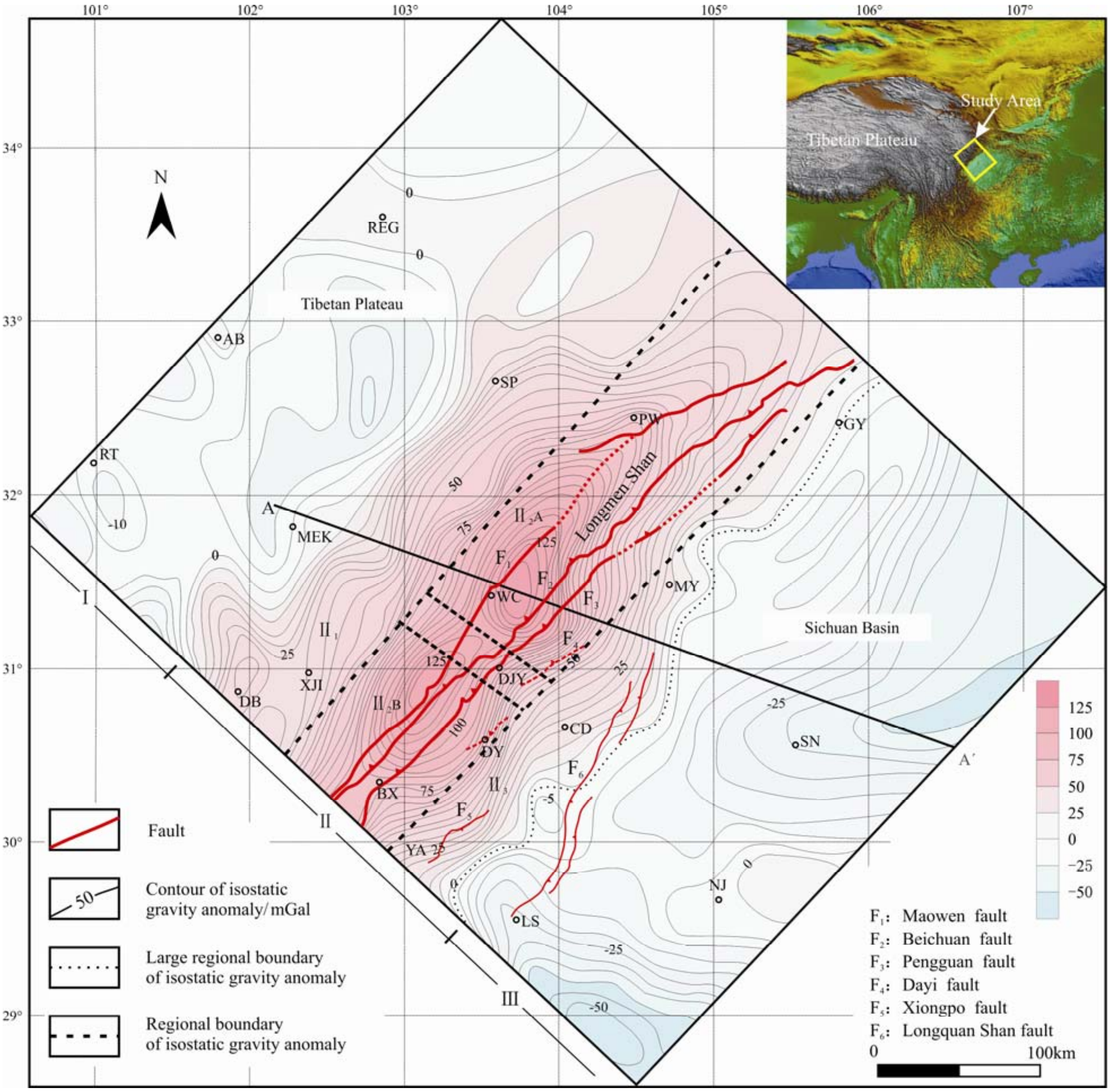

Fig. 3. IGA map of the eastern margin of the Tibetan Plateau in accordance with Airy's isostasy model.

The raw gravity data comes from GPTSBGMR, who got the data with the accelerometer in 1988. The map (the scale is 1: 3,000,000, the precision of the isostatic gravity anomaly is 2×10^{-5} m/s^2, and contour interval is 5×10^{-5} m/s^2) was plotted based on correcting the raw gravity data (the scale is 1: 1,000,000) with global altitude, middle layer, topography, normal field, and isostatic corrected according to Airy model. I=weakly negative IGA zone in the Tibetan Plateau; II=positive IGA zone in LMS; III=negative IGA zone in Sichuan Basin. Original data from Li Yong et al. (1995, 2005), Liu Shugen (1993) and Wang Qianshen et al. (2008). F_1=Maowen Fault; F_2=Beichuan Fault; F_3=Pengguan Fault; F_4=Dayi Fault; F_5=Xiongpo Fault; F_6=Longquan Shan Fault; CD=Chengdu; MY=Mianyang; YA=Ya'an; GY=Guangyuan; SP=Songpan; MEK=Maerkang, SN=Suining

shows:

(i) The IGA values are smaller than the Bouguer anomalies, with less variation, and are independent of topography. In other words, the gravity effects of topography and crust thickness are eliminated, thus highlighting information about tectonic changes taking place in the crust. The IGA map therefore explains the dynamic processes in the crust more effectively.

(ii) According to Airy's isostasy theory, larger IGA values indicate greater buoyancy forces in the crust. If IGA values is less than or close to zero, the crust is close to a state of isostatic equilibrium. Specifically, if the anomaly is positive, downward isostatic subsidence is taking place in the region, and accordingly the height of the topography (H) is decreasing and the crust is tending toward isostatic equilibrium. If the anomaly value is negative, upward isostatic lifting is taking place in the region, and H will increase accordingly as the crust tends toward a state of isostatic equilibrium.

(iii) The IGA values over the whole region present a variation pattern of negative-zero-positive maximum-zero-negative from northwest to southeast, and may be divided into a weakly negative IGA zone in the Tibetan Plateau (zone I in Fig. 3), a positive IGA zone in the LMS (II), and a negative IGA zone in the Sichuan Basin (III).

4.2 Correlation between IGA zones and tectonic landform units

To study the relationship between tectonic landform units and IGA, the IGA map was compared with tectonic, surface rupture, and aftershock maps from the Wenchuan and Lushan Earthquakes. The results are shown in Fig. 3 and Fig. 5–8, from which several conclusions can be drawn:

(1) The system at the eastern margin of the Tibetan Plateau correspond to the three IGA zones as outlined above: the eastern Tibetan Plateau, the LMS orogenic belt, and the Chengdu Basin (western Sichuan Basin) at the western margin of the Yangtze Plate systems). We suggest that the IGA zones correspond to tectonic landform units, and the zonation of the IGA data primarily reflects the tectonic landform units at the eastern margin (Fig. 5).

(2) The high positive IGA zone corresponds to the LMS orogenic belt, with its distinctive seismic risks and high-mountain topography. In this region, the IGA value, ranging from 0 to 125 mGal, conforms to the trend of the LMS orogenic belt striking northeastward. In addition, two oval-shaped regions with abnormally high positive IGA values up to 125 and 135 mGal can be observed within the LMS. The northern oval-shaped region (zone IIA in Fig. 3; Fig. 6a; Fig. 6b) corresponds to the aftershock zones of the 2008 Wenchuan Earthquake. The southern oval-shaped region (zone IIB in Fig. 3; Fig. 6a; Fig. 6b) corresponds to the aftershock zones of the 2013 Lushan Earthquake. These results indicate that the LMS may be subdivided into northern and southern segments. The boundary between them may be a northwestward transverse fault or a tear fault that extends from Lixian City to Dujiangyan City.

(3) The northwestern weakly negative IGA zone corresponds to the eastern Tibetan Plateau, with flat topography an average elevation of about 4 km and IGA values ranging from –10 to –20 mGal. The shape of the IGA contours encircling the low-value points are not parallel to the strike of the LMS, indicating that the region is in a relatively stable isostatic state of overall uplift, with little neotectonic activity. The block is composed of epimetamorphic rocks of the Indosinian Songpan–Ganzi orogenic belt more than 7 km deep, with multilayered detachment and thrust faults (according to data from the Hongcan 1 well drilled by Sinopec). The epimetamorphic rocks are made up of Middle and Lower Triassic flysch, are regarded as the sedimentary record of a Late Triassic remnant ocean basin (Li et al., 2003), and have experienced strong tectonic deformation. During the Mesozoic, the block has undergone three stages of tectonic shortening (Simon et al., 2003) but was comparatively stable during the Cenozoic, during which it underwent uplifting with no tectonic shortening. The large-scale detachment fault (Xu Zhiqin et al., 2007) or the Maowen Shear Zone (Liu Shugen, 1993) is assumed to be the boundary between the block and the LMS.

(4) The southeastern, weakly negative IGA zone corresponds to the Sichuan Basin located at the western margin of the stable Yangtze Plate, where the IGA values range from 0 to –50 mGal. This suggests that the crust in this region is in a comparatively stable isostatic state, and that neotectonic movement has been characterized by regional uplift and denudation. At least 1–4 km of strata thickness in the basin has been eroded in the past 40 Ma

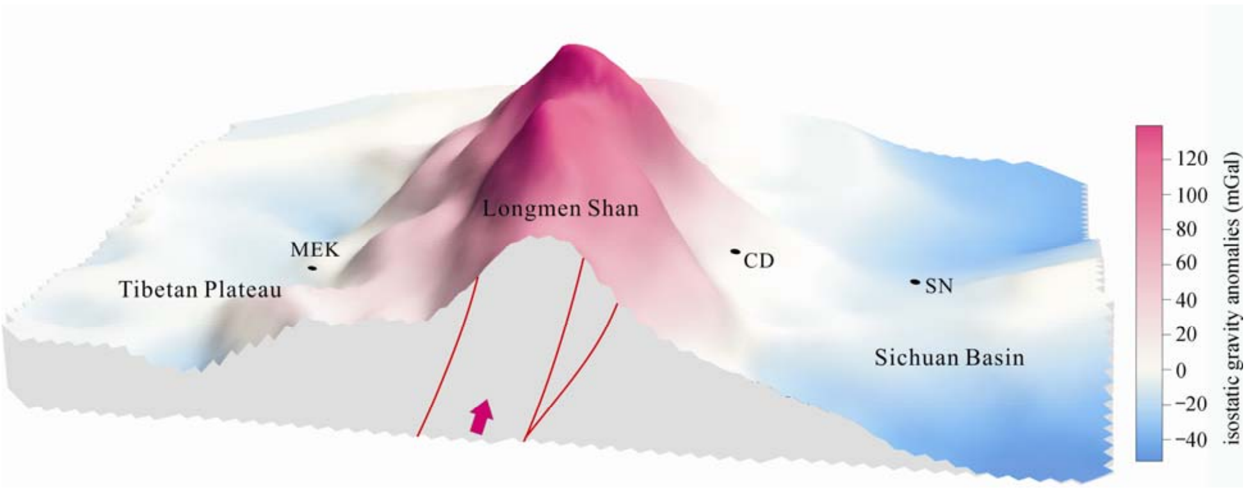

Fig. 4. 3D IGA(mGal) map of the eastern margin of the Tibetan Plateau according to Airy’s isostasy model.
The map was plotted by Surfer 8.0 software based on the data of isostatic gravity anomalies from Fig. 5. CD=Chengdu; SN=Suining; MEK=Maerkang

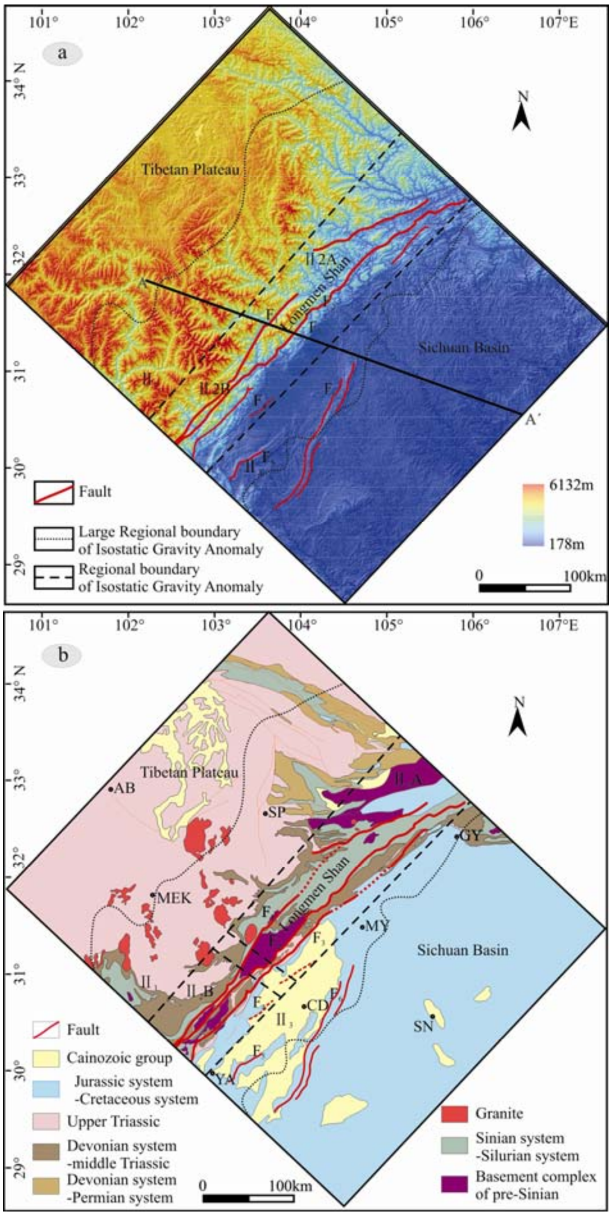

Fig. 5. (a) Comparison between IGA map and geomorphological units (data selected from the SRTM 90 m digital elevation data). The abrupt change-zone from positive IGA values corresponds to a zone of abrupt topographical changes; (b) Comparison between IGA map and geological units. The positive IGA zone corresponds to the LMS orogenic belt.

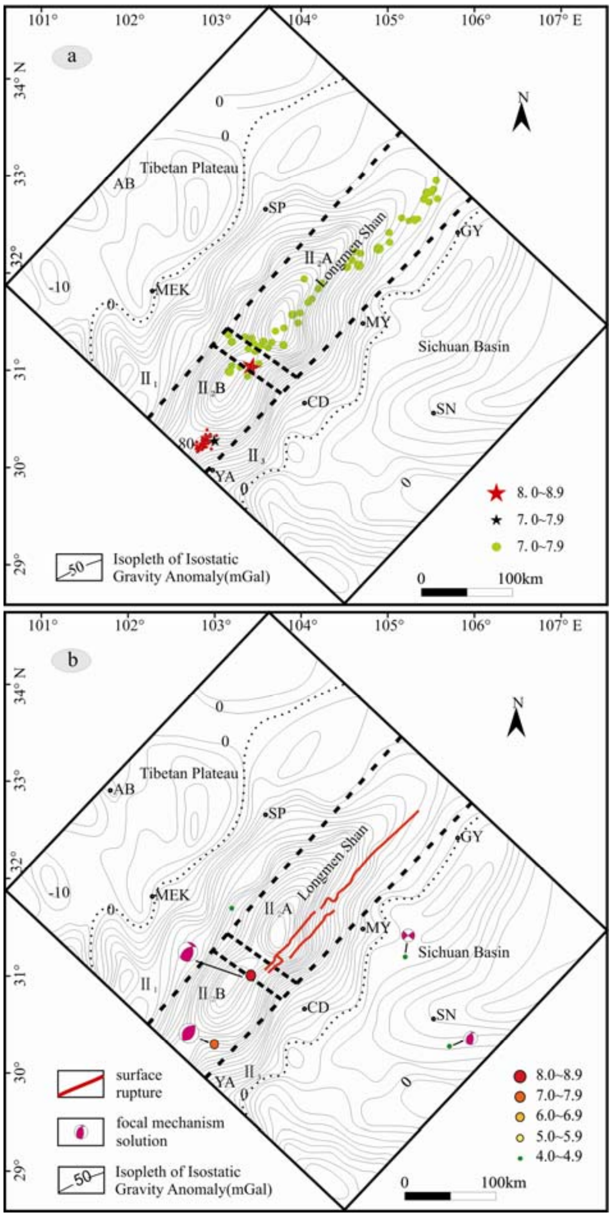

Fig. 6. (a) Comparative map of IGA values and aftershocks following the Wenchuan and Lushan Earthquakes. Both earthquakes and related aftershocks occurred along the belt with abrupt changes in positive IGA values on the front edge. (b) Comparative map of IGA values and surface rupture zones following the Wenchuan Earthquake. Surface rupture zones of the earthquake occurred along the belt with abrupt changes in positive IGA values on the front edge.

(Richardson et al., 2008). Seismic reflection profiles indicate that the strata in the Sichuan Basin are flat and consist of basement rocks overlain by approximately 10 km of Paleozoic and Mesozoic sedimentary rocks. The rocks cropping out at the surface are mainly Jurassic, Cretaceous and Cenozoic clastics. A series of anticlines and synclines with a northeasterly strike alternate throughout the western Sichuan Basin. From northwest to southeast, these are the LMS foothills, the Chengdu Basin (syncline), the Xiongpo anticline, the Longquan Mountain anticline, the Weiyuan anticline, and the Huaying Mountain folds. In addition, the strata exhibit a regional westward dip of 2–3 towards the LMS west of the Weiyuan anticline. This dip may be related to loading of the crust by the mountain belt (Hubbard and Shaw, 2009). The six major structural trends are formed by fault-bend or fault propagation folds rooted in detachments that transfer shortening from the mountain belt towards the east into the Sichuan Basin (Hubbard and Shaw, 2009). These results suggest that relatively little tectonic shortening deformation has taken place in the Sichuan Basin since the Cenozoic.

Note that the IGA in the Sichuan Basin vary slightly. Specifically, in the western part of Longquan Mountain, the IGA values are positive but they are negative to the east which, according to the Airy model, would suggest downward isostatic subsidence west of Longquan Mountain and isostatic uplift to the east. In addition, zones of extremely low IGA values, ranging from –40 to –50 mGal, have been detected along the Weiyuan anticline. The shape of the contour lines of the IGA values encircling the low-value points are sub-parallel to the strike of the LMS, suggesting that the low values are related to loading of the crust by the mountain belt.

4.3 Correlation between abrupt IGA changes belt and steep topography

To investigate the relationship between steep topography and IGA values, the IGA map was compared with the topographic relief map. The results are shown in Fig. 5 and Fig. 7, from which we draw the following conclusions.

From northwest to southeast, the region consists of three primary geomorphological units: the Tibetan Plateau, the mountainous region in the LMS and the Sichuan Basin, as shown in Fig. 5a. There is an abrupt change of slope, marked by steep topography, between the LMS and the front region (Densmore et al., 2005, 2007) with an elevation difference greater than 4500 m. The steep topography corresponds to the abrupt IGA changes from 75 to 125 mGal at the front edge of the LMS (Fig. 7a), as shown in Fig. 6c. The larger IGA values correspond to greater elevation, implying that the zone of sharp topographic change may be a primary factor causing the abrupt change in IGA values at the eastern margin of the Tibetan Plateau.

4.4 Correlation between the changes of IGA and rock density

A large area of Precambrian Pengguan and Baoxing Complexes cropping out along the LMS is composed of a series of basic, neutral and acid-intrusive rocks (Fig. 5b; Fig. 7b). These complexes have been faulted and cut into several thin imbricated tectonic sheet-like slices. In order to study the relationship between IGA values and rock density, the IGA values were compared with the density of the Precambrian complexes, metamorphic rocks and sedimentary rocks. The results are shown in Fig. 3 and Fig. 8, from which we draw several conclusions:

(1) The IGA values are related to the density of the surface rocks. Specifically, areas with high positive IGA values correspond to the areas of the Pengguan and Baoxing Complexes. The density varied from 2.56 to 3.02 g/cm^3, with an average of 2.80 g/cm^3 (Hu Yuanxin et al., 2010). Areas with low or negative IGA values correspond to the areas of exposed high-density epimetamorphic rocks (density 2.66–2.72 g/cm^3, average 2.69 g/cm^3 (Liu Beili, 1994) and sedimentary rocks (density 2.60–2.80 g/cm^3, average 2.68 g/cm^3 (Liu Beili, 1994)). These figures indicate that the high-density Pengguan and Baoxing Complexes are the primary factors causing positive IGA

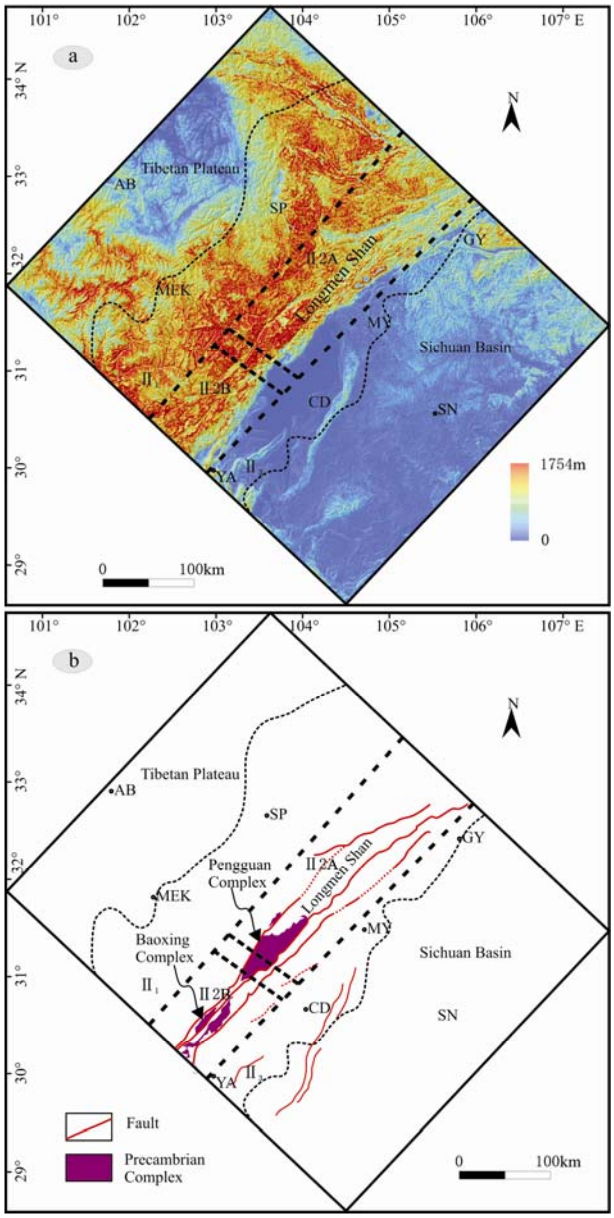

Fig. 7. (a) Comparative map of IGA values and topographical relief. The belt with abrupt changes in positive IGA values corresponds to the belt of abrupt topographical changes. (b) Comparative map of IGA values and distribution of the Precambrian complex. Points of high positive IGA values in the LMS correspond to surface outcrops of the Pengguan and Baoxing Complexes.

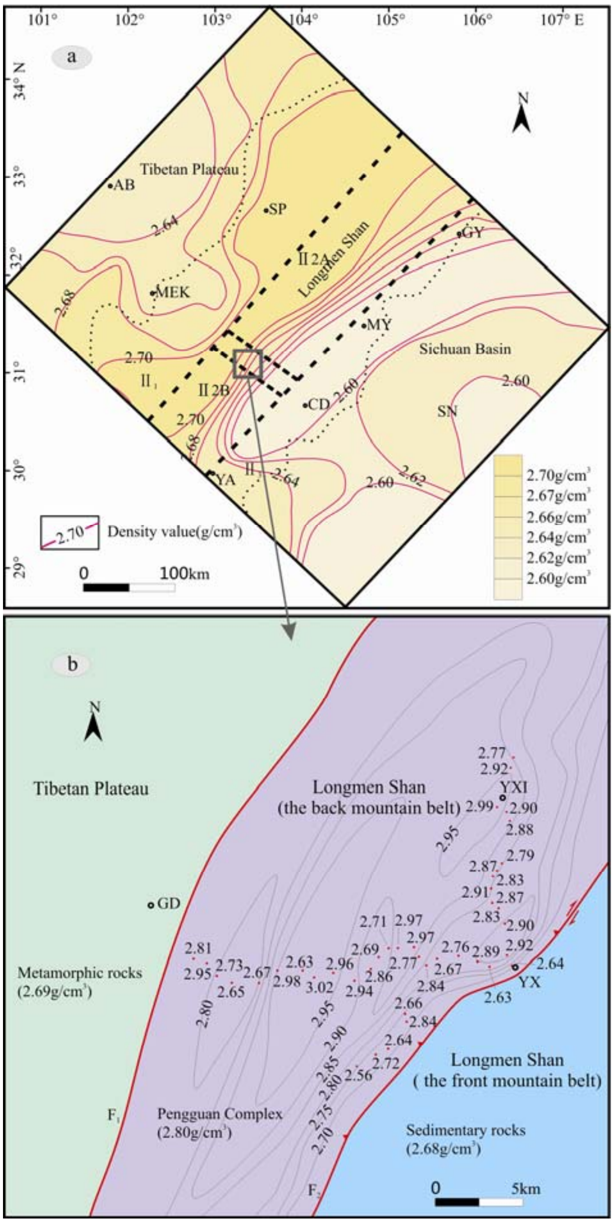

Fig. 8. (a) Comparative map of IGA and surface rock density contours (original data from Liu, 1994). High positive IGA belt in the LMS corresponds to high-density rocks Pengguan and Baoxing Complexes; weakly negative zones correspond to sedimentary and epimetamorphic rocks. (b) Measured data for surface rock density (original data from Hu Yuanxin et al., 2010).

Average density of the Pengguan Complex along the LMS=2.80 g/cm^3; average density of epimetamorphic rocks in eastern Tibetan Plateau=2.69 g/cm^3; average density of sedimentary rocks in Sichuan Basin=2.68 g/cm^3.

zones.

(2) Zones with abrupt changes in IGA values correspond to zones of abrupt change in rock density. The difference in the densities of the Pengguan Complex rock along the LMS and of the sedimentary rocks in the Sichuan Basin is greater than 0.12 g/cm^3 (2.80 g/cm^3–2.68 g/cm^3) suggesting that density differences are responsible for the abrupt changes in IGA values. These gravity anomalies induced by the density differences are quite important when considering vertical uplift of the LMS.

(3) The high-density Pengguan and Baoxing Complexes originated from the lower crust, indicating that density loading is one of the most prominent characteristics of the present LMS. Consequently, we suggest that upward extrusion and uplift of lower crustal flow has pushed high-density lower crustal materials into the upper crust, thus increasing the density of the LMS.

5 Simulation of IGA Using Airy Isostasy Model

5.1 Airy isostasy model and the simulation method

According to the Airy isostasy model, IGA values in a given region reflect the current isostatic state. A non-equilibrium state will inevitably lead to the generation of isostatic movements. Because isostatic movements occur in the high-density, highly viscous liquid layer, the rate of isostatic recovery is slow, continuing over very long geological time periods. The measured IGA values lead to the inference that the eastern Tibetan Plateau is almost in a state of isostatic equilibrium, or isostasy, and exhibits no discernible isostatic uplift. The LMS, being located in a positive IGA zone, shows evidence of isostatic subsidence. The Sichuan Basin exhibits negative IGA, evidence of isostatic uplift.

The Airy isostasy model proposes that the mountain float in the liquid layer with high density. The isostatic compensation areas depend on the depth of the upper layer, and the height of the mountain is offset by a deep root. This is expressed by:

$$h_{root}=h_{mt}\rho_1/(\rho_2-\rho_1) \quad (1)$$

where h_{root} is the thickness of the mountain root; h_{mt} is the height of the mountain above ground surface; ρ_1 is the density of the upper layer above the isostatic compensation area; and ρ_2 is the density of the layer beneath the isostatic compensation area.

Substituting in Eq. (1) the values ρ_1 (i.e., the average density of the rocks above the Moho)=2.85 g/cm^3, and ρ_2 (i.e., the average density below the Moho)=3.40 g/cm^3, gives:

$$h_{root}=5.18h_{mt} \quad (2)$$

Currently, the elevation of the LMS (h_{mt}) is 5 km. According to Eq. (2), the Moho surface would be deformed by a downward root with compensation thickness (h_{root}) of 25.9 km. However, the densities calculated from the measured thickness (Fig. 9) indicate that the current mountain root below the Moho discontinuity (h_c) is only 5 to 7 km (Luo et al., 1994; Wang Qianshen et al., 2008), which is far less than the thickness of isostatic compensation. Therefore, the LMS is characterized by positive IGA. Based on the density calculated from the measured depth profile (Fig. 9), the Moho discontinuity in the LMS is undergoing isostatic subsidence, and will continue to subside for a further 18.9 km, according to the Airy isostasy model. Topographical relief data shows that the LMS, in particular Jiuding Mountain, is currently rising at the rate of 0.3–0.4 mm/yr (Liu Shugen, 1993). Consequently, the LMS must be subject to an uplift force which exceeds the isostatic adjustment force. To perform in-depth investigations into the accessional range induced by the uplifting force, simulations and inversions of the positive IGA were conducted along the A–A' profile (Fig. 10) in Fig. 3. With

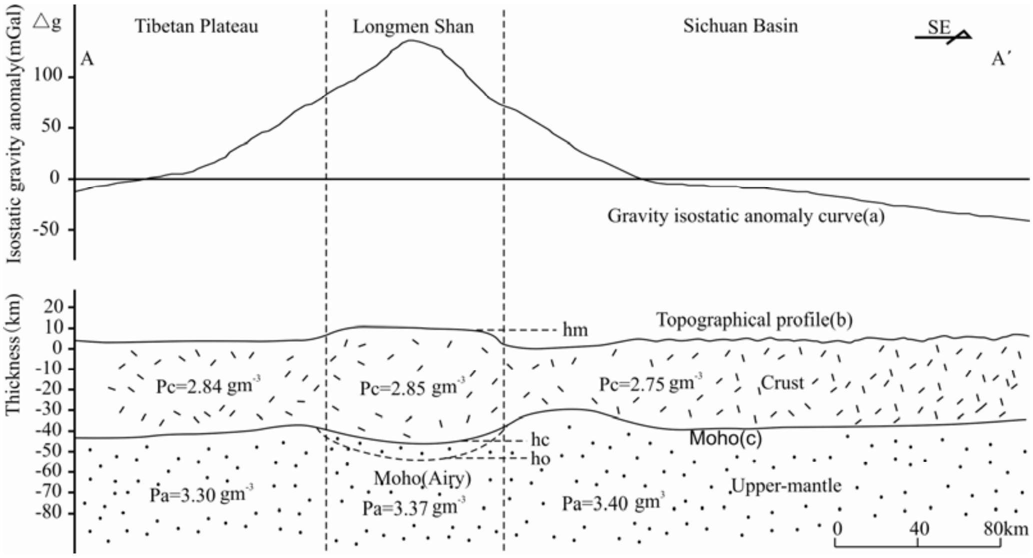

Fig. 9. Simulations and related interpretation of IGA values at the eastern margin of the Tibetan Plateau according to the Airy isostasy model.
IGA curve from Fig. 2; topographical profile from digital elevation map; burial depth and density of Moho surface from Wang Qianshen et al. (2008).

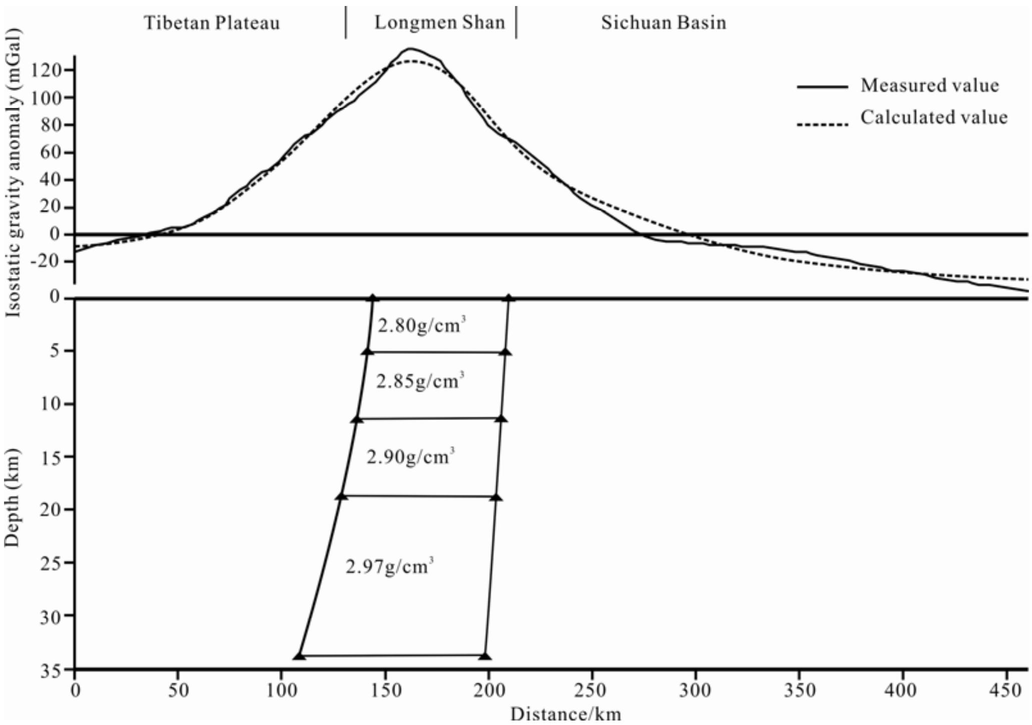

Fig. 10. Inversion of the IGA profile (section A–A', Fig. 2) on the eastern margin of the Tibetan Plateau, from the calculation of gravity anomalies of 3D bodies.
With the velocity profile developed from deep seismic sounding (GPTSBGMR, 1991), the density profile can be determined and based on the density profile, the lithosphere could be divided into at least four layers: the upper crustal layer (the sedimentary cover), middle crustal layer, lower crustal layer, and the upper layer of the mantle.

the velocity profile developed from deep seismic sounding (GPTSBGMR, 1991), we were also able to determine the density profile (Fig. 10). Based on the density profile, the lithosphere could then be divided into at least four layers: the upper crustal layer (the sedimentary cover), middle crustal layer, lower crustal layer, and the upper layer of the mantle.

The initial model and the density values for generating the IGA values were calibrated from the depths and densities of each layer (GPTSBGMR, 1991). The IGA values, the relevant simulated structure and the density values were then used to calculate three-dimensional gravity anomalies. The IGA values were calculated and compared with the input anomaly map (Fig. 10). By constantly modifying the shape and burial depth of the simulated body by trial and error, the two curves were matched as closely as possible (i.e., the mean squared prediction error between the two curves was minimized). Finally, the parameters of the best-match simulation body were selected as the geological parameters of the IGA values in the profile, thus simulating the vertical profile and related parameters characterizing the unequal densities in this region (Fig. 10). In this way, the burial depth, the central burial depth and the width at the top of the upper mantle in the simulated body were obtained. In addition, a morphology was proposed for the IGA values generated by the geological body at different depths, and vertical variations were deduced from the observed IGA values. The mean square error of the simulations was 6.9 mGal.

5.2 Simulation results

5.2.1 Crustal structure of LMS and boundary faults

The blocks in the simulations consisted of four horizontal layers of different density (Fig. 10; Fig. 11): the lower crustal layer (2.97 g/cm^3), the middle crustal layer (2.90 g/cm^3), the lower part of the upper crustal layer (2.85 g/cm^3) and the upper part of the upper crustal layer (2.80 g/cm^3). The bounding faults on the eastern and western sides of these blocks were sub-vertical, tilted slightly towards the west to simulate the front and rear faults of the LMS inclined towards the northwest are high-angle faults rather than low-angle overthrust faults. The LMS at depth was displaced slightly towards the northwest relative to the surface to suggest that, as a whole, it dips towards the northwest. In particular, the mountain lacks a root, being instead an independent intracontinental tectonic loading system. The rear fault, corresponding to the Maowen Fault at the surface, has also been termed by Xu Zhiqin et al. (2007) as the “large-scale detachment fault on the eastern margin of the Tibetan Plateau” (ETD), or “the Maowen shear zone” (WMSZ) by Liu Shugen (1993). Thus the model suggests that the

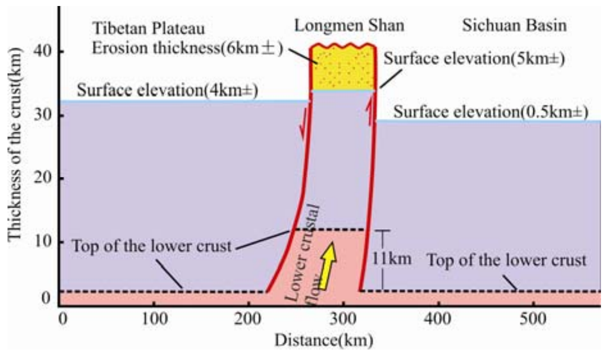

Fig. 11. Uplift of lower crustal flow, surface uplift, and denudation along the LMS at the eastern margin of the Tibetan Plateau

Longmen Shan fold belt and the Songpan–Ganzi fold belt are two different geological bodies separated by the rear (Maowen) fault. ^{40}Ar-^{39}Ar dating of biotite has given an age of approximately 112–120 Ma, suggesting that this fault with extension dominates was formed around 120 Ma (Burchfiel et al., 2008; Xu Zhiqin et al., 2007). The front fault, which corresponds to the Pengguan Fault at the surface, is the boundary between the LMS and the extension deformation belt in front of the mountain.

5.2.2 Uplift of the top of the lower crust in the LMS and lower crustal flow

As shown in Fig. 9 and Fig. 10, the top of the lower crust (density of 2.97 g/cm^3) lies at a depth of only 19 km, whereas the depth of the top of the lower crust beneath the Tibetan Plateau (density varying from 0 to –20 mGal) is more than 30 km. The difference is about 11 km; that is, the top of the lower crust, as inferred from the positive IGA zones along the LMS, has been raised 11 km above the areas that do not show anomalous gravity data. This conclusion is of great significance, as is made clear in the following.

We all known that surface uplift and uplift of rock cannot be equal, and the relation between these two displacements is: surface uplift=uplift of rock−exhumation (e. g. England and Molnar, 1990). So, the surface uplift magnitude of the LMS is mainly affected by two factors: crustal uplift magnitude and the erosion thickness of the corresponding period.

First, suppose that the surface was uplifted 11 km, as above; however, the maximum surface elevation in the LMS is currently 5 km, implying that a depth of approximately 6–7 km has been eroded. This is consistent with low-temperature thermochronology results of Xu and Kamp (2000) suggesting that at least 6–10 km of crustal thickness has been denuded since the Cenozoic, evidence that the simulation methods and the results obtained in the present work are reliable.

Second, the positive IGAs indicate that the lower crust has been vertically uplifted. Because this is confined to the LMS, we propose that in addition to shortening and extrusion, lower crustal flow has contributed to the 11 km uplift (Fig. 11) and that such an uplift force could have disturbed the isostatic state of the LMS.

Third, uplift of lower crust material along the LMS would have been hindered by the solid crust of the Sichuan Basin, forcing it to move vertically. High-density materials in the lower crust would eventually accumulate in the LMS, giving rise to the extrusive lower crust and the steep topography of the LMS. This scenario explains why the areas with high IGA values and tectonic shortening are apparent only along the LMS orogenic belt. It is well supported by the nappes, klippes and thrust faults observed in the LMS. By contrast, the eastern parts of the Tibetan Plateau are relatively stable and show little or no evidence of tectonic shortening, with a low horizontal shortening rate of approximately 1–3 mm/yr measured by GPS techniques (Chen et al., 2001; Zhang et al., 2004). The horizontal extrusion of the lower crustal flow at the front edge of the LMS would lead to folds and unconformities at the base of the frontal foreland basin (western Sichuan Basin). Therefore, we conclude that tectonic shortening driven by lower crustal flow is confined to the LMS and its front edge, and is not part of a continuous crustal shortening of the whole of the eastern Tibetan Plateau. This type of tectonic shortening is therefore defined here as “limited tectonic shortening”.

5.2.3 Simulation of tectonic loading in the LMS and flexural subsidence in the foreland basin using flexural isostasy models

The Airy isostasy theory proposes that if the LMS were in isostatic equilibrium, the thickest crust would occur beneath the eastern margin of the Tibetan Plateau. According to the theory, the higher the mountain is above the surface, the deeper must be its root and therefore the thicker the crust. In fact, however, this is not the case. The GPTSBGMR (1991) finished an unpublished report, which tell us the information about the Moho. The steep of Moho in Tibetan Plateau, LMS and Sichuan Basin are 56–66 km, 46–56 km and 42–46 km respectively in this unpublished report. Wang Qianshen et al. (2008) give us the latest data: The steep of Moho in Tibetan Plateau, LMS and Sichuan Basin are 56–60 km, 45–50 km and 40–43 km respectively. These two data are very similar, so we choose the latest data in this paper. The LMS is located in a zone where crustal thickness to the northwest abruptly increases to approximately 56–60 km, whereas in the Sichuan Basin in the southeast it is approximately 40–43 km (Wang Qianshen et al., 2008), and only 45–50 km thick beneath the LMS (Wang Qianshen et al., 2008). Obviously, then, the variation in crustal thickness in the region cannot be explained by Airy’s isostasy theory.

In the present work, the flexural isostasy model of Watts (1992) was adopted to account for the observed phenomena. Although based on Airy’s isostasy theory, the Watts model suggests that the superimposed load also causes the solid crust to bend elastically. The compensatory masses are thus distributed both vertically and horizontally over a large region. The variation of IGA values from west to east tends to be negative-zero-maximum then positive-zero-negative, suggesting that regional compensation is taking place at the eastern margin of the plateau. The positive IGA values observed at the LMS are offset by elastic flexure of the crust in the Sichuan Basin.

Coupling mechanisms were once believed to link the tectonic loadings in the LMS and the flexural subsidence in the foreland basin (Li et al., 2003, Yan Zhaokun et al., 2016). The width and depth of the foreland basin are related to the size and morphology of the thrust wedges, and to the flexural rigidity and thickness of the lithosphere. In the present work, the Watts model was adopted to quantitatively calculate the tectonic load of the LMS, the flexural subsidence of the foreland basin, the elastic thickness (T_e) and the flexural wavelength from observed IGA values. The flexural subsidence generated in the elastic plates by the tectonic loadings was then simulated using one-dimensional analysis.

5.3 Tectonic load in the LMS

As discussed, the zones of positive IGA are found only in the LMS orogenic belt, from which it is inferred that it is only the LMS that exhibits intensive tectonic and density loading along the eastern margin of the Tibetan Plateau (Fig. 12). In the present study, this region is defined as “a narrow tectonic load belt”, in which the tectonic load is distributed in a narrow zone, or belt, between the Maowen and Pengguan Faults. The volume of tectonic load is limited i.e., not on a large scale, unrelated to a vast orogenic wedge, and does not cover the whole eastern part of the plateau. The positive IGA values reflect the difference between the theoretical crustal thickness when in isostatic equilibrium (approximately 50 to 60 km), and the actual crustal thickness (approximately 45 to 50 km) (Wang Qianshen et al., 2008). This difference (5–10 km) between theoretical crustal thickness and actual crustal thickness is here regarded as the thickness of the tectonic load in the LMS. Therefore, adopting the location and thickness data in Fig. 3 the regions regarded as being subjected to tectonic load in the LMS are those regions where the IGA values vary from 75 to 125 mGal (Fig. 10).

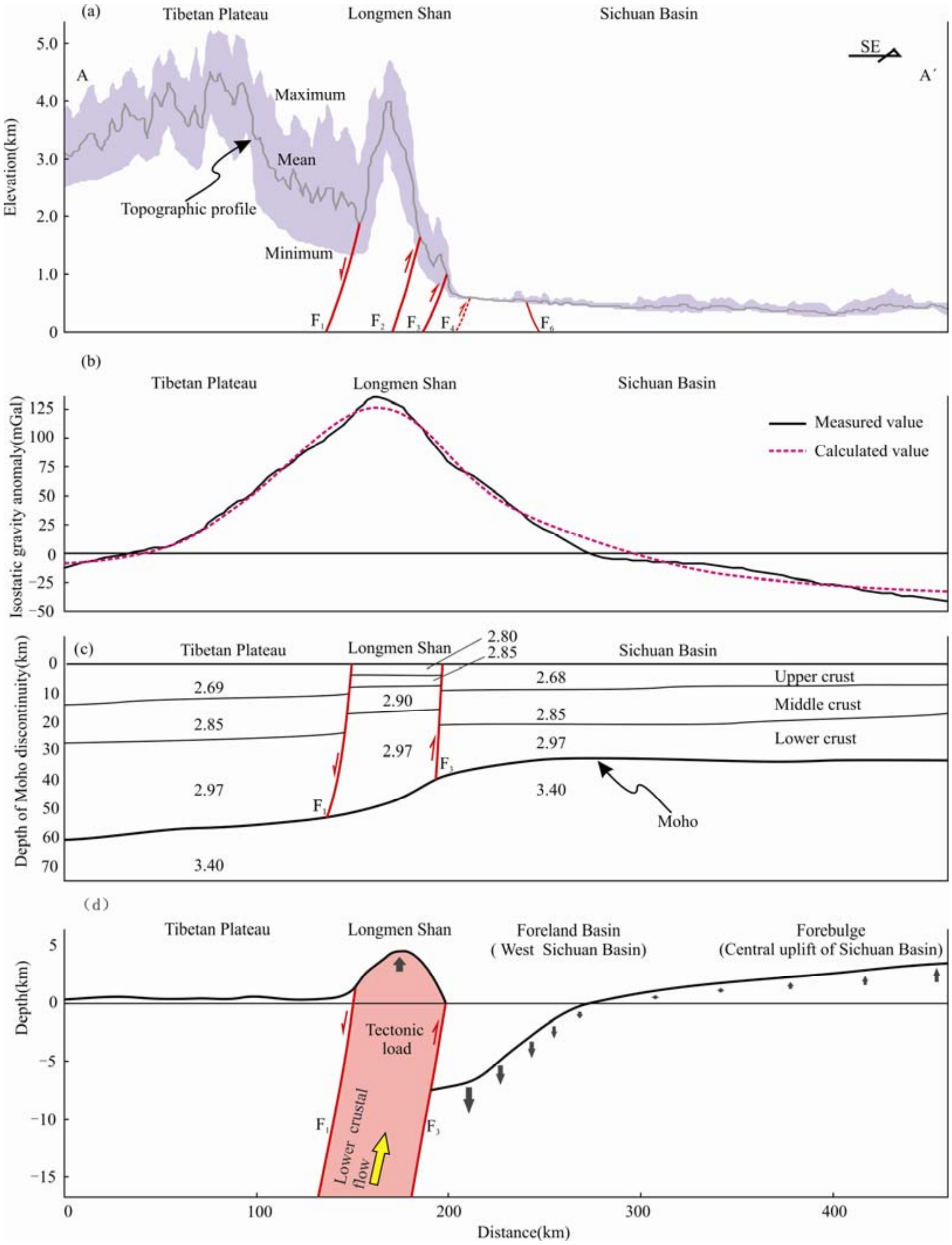

Fig. 12. Tectonic load in LMS and flexural subsidence in the foreland basin revealed by IGA values on eastern margin of Tibetan Plateau.

(a) A–A' topographic profile (Fig. 2): average height from profile, width 10 km, length 460 km. Source: SRTM database at a height of 90 m; (b) A–A' IGA profile and simulated profile; (c) crustal depths along A–A' and density profile (g/cm^3), the data from the GPTSBGMR(1991); (d) tectonic load in LMS and flexural subsidence in foreland basin. Amplitude of flexural subsidence and flexural uplift in forebulge obtained from IGA values

Using software Surfer 8.0, and taking the values of average density as 2.80 g/cm^3, volume 1.8×10^5 km^3, area 1.9×10^4 km^2 and average thickness 9.46 km, the tectonic load (V_p) in the LMS was calculated to be 5.08×10^{14} t.

5.4 Isostatic subsidence in the foreland basin

As shown in Fig. 3 the western part of the Sichuan Basin is characterized by positive IGA values (0–75 mGal), which decrease to zero at Longquan Mountain. The crust in positive IGA zones exhibits downward isostatic subsidence. A positive IGA value denotes the difference between the theoretical isostatic crustal thickness (40–43 km) and the actual crustal thickness (39 km) (Wang Qianshen et al., 2008), which is therefore between 1 and 4 km. This difference is viewed as the depth of isostatic subsidence in the basin. Accordingly, based on the location and depth data shown in Fig. 3 the regions where positive IGA values vary from 75 to 0 mGal are regarded as foredeep. Flexural subsidence of the foredeep was calculated using Surfer 8.0 software, with results are shown in Fig. 13.

5.5 Uplift of the forebulge

As shown in Fig. 3 the IGA values are negative to the east of Longquan Mountain in the Sichuan Basin, gradually increasing eastward to −30 mGal in the central uplift of the Sichuan Basin, and form a trap of negative IGA values. The crust in this region is characterized by isostatic uplift. Negative IGA values reflect the difference between the theoretical crust thickness (40–43 km) and actual crustal thickness (39 km) (Wang Qianshen et al., 2008). The difference of 1 to 4 km is regarded as the amplitude of flexural uplift. According to the location and thickness data in Fig. 3 regions of negative IGA from 0 to –30 mGal are regarded as the forebulge. The uplift values shown in Fig. 13 were calculated using Surfer 8.0 software.

5.6 Simulation of elastic flexure

The lithosphere in this region was simulated as an elastic block of specific density and effective elastic thickness (T_e) overlying a viscous layer. The stress deviation in the viscous layer was reinforced during the tectonic loading process. From the tectonic loading values calculated for the LMS, together with the subsidence in the foreland basin, the uplift in the forebulge and the sediment load in the Chengdu Basin (sediments less than 541 m thick since 3.6 Ma), the elastic flexure was calculated using the conventional elasticity equation for linear loads on an elastic foundation (Hetenyi, 1974):

$$\omega = \frac{H}{2\alpha(\rho_m - \rho_a)g}\exp\left(-\frac{x}{a}\right)\left(\cos\frac{x}{a}+\sin\frac{x}{a}\right) \tag{3}$$

where ω is elastic flexure; H is tectonic load (stress per unit length); ρ_m is the density of the mantle (3300 kg/m^3); ρ_a is air density (1 kg/m^3); g is acceleration due to gravity (9.8 m/s^2); x is the distance from the load; and α is an flexural parameter for calculating T_e. To constrain the selected T_e, flexural profiles for T_e ranging from 25 to 55 were calculated. The results indicate:

(1) As shown in Fig. 13, the flexural profile is a typical foreland basin, exhibiting a foredeep (which is located between 0 and 75 km from the LMS) and a forebulge (which is remote from the LMS, 75–125 km distant). The data suggests that the near-end flexural subsidence in the foreland basin, and the far-end uplift of the forebulge (the central uplift in the Sichuan Basin), are caused by the tectonic loading in the LMS.

(2) With increasing T_e, the regions with maximum and minimum areas of flexural subsidence at the front edge of the LMS shift towards the Sichuan Basin. An obvious subsidence region is observed in the western Sichuan Basin. The amount of subsidence decreases gradually towards the southeast. Uplift occurs in Longquan Mountain and eastward (the simulation curves show a mild uplift at 75 km); that is, the uplift of the forebulge.

(3) The flexural profile is similar to the subsidence profile in Fig. 13, suggesting a typical foreland basin–forebulge system. The best match between the simulated curve and the subsidence profile from the IGA values was obtained when the flexural parameter was assigned the value 25 km; therefore T_e=25 km was regarded as the ideal elastic thickness.

(4) The volume of the narrow tectonic load in the LMS

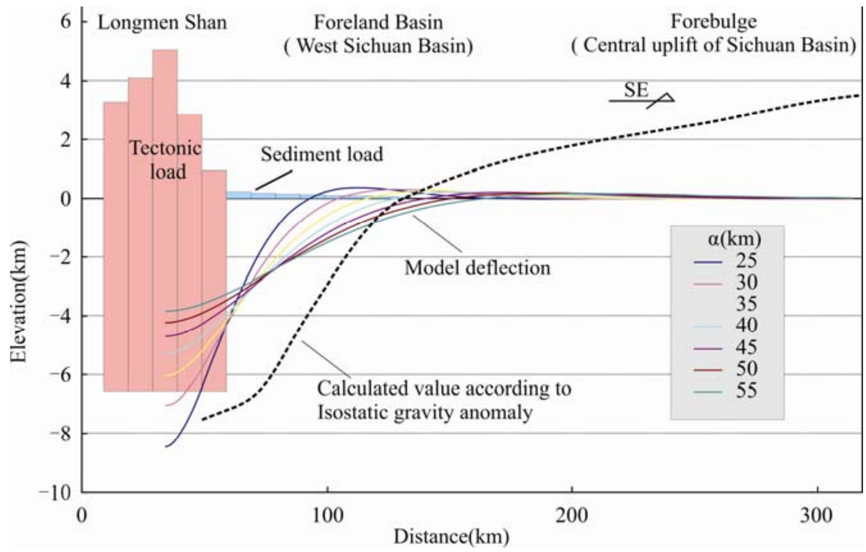

Fig. 13. Simulation of tectonic loading in LMS and flexural subsidence in foreland basin.

is only 1.8×10^5 km^3. This lies between 2.6±1.2 km^3 (the estimated volume of the Wenchuan Earthquake (de Michele et al., 2010) and 5×10^{23} km^3, which is the estimated volume involved in the Indosinian movement (Li et al., 2003). This volume is not sufficient to initiate large-scale, large-amplitude flexural subsidence and form a large-scale, wedge-like foreland basin. But it could drive a small-scale, wedge-like foreland basin with characteristics such as narrow width (less than 75 km), small accommodation space (with thickness less than 541 m), and asymmetrical subsidence. We suggest that the present small foreland basin (i.e., the Chengdu Basin) is quite different from the large wedge-like foreland basins induced by large-scale tectonism such as that which formed foreland basins in the Upper Triassic (Li et al., 2003).

6 Discussion

6.1 Relationship between lower crustal flow and positive IGA in LMS

The uplift of the LMS has been explained by lower crustal flow or extrusion mechanisms (Royden et al., 1997; Simon et al., 2003; Xu Zhiqin et al., 2007; Wang et al., 2012). The results of the present study indicate that the IGA values in the LMS are positive. We have studied the relationship between the high, steep topography and the IGA data, and between the positive IGA values and lower crustal extrusion in the LMS, and concluded that the positive IGA values in the LMS reflect uplift due to lower crustal flow.

The vertical uplift in the LMS is estimated to be have been 11 km, and is a significant factor in the deformation of the Moho topography and in the crustal structure at the eastern edge of the Tibetan Plateau. By investigating the relationship between IGA values and elastic thickness, we conclude that the flexure is related to lower crustal flow beneath the eastern edge of the plateau. We suggest that the lower crustal flow beneath the plateau moves eastward until it is obstructed by the solid base of the Sichuan Basin. This has led to sub-vertical extrusion in the LMS and sub-vertical movement of lower crustal materials. The limited tectonic shortening, tectonic loading and density loading driven by the lower crustal flow along the LMS has produced flexural subsidence in the foreland basin.

6.2 Relationship between lower crustal flow and the Wenchuan Earthquake

Seismic data (e.g., focal mechanism data, earthquake history, surface rupture zone distribution during the Wenchuan Earthquake and aftershocks) has been correlated with the belt of abrupt IGA changes in the LMS. From these data we conclude the following.

(1) Strong earthquakes of magnitude greater than Ms 6.0 have all occurred in the belt of abrupt changes in IGA. That is, this zone is tectonically active and breeds earthquakes; however, to the west and east of this belt, as symptomized by zones of weak IGA, the frequency and intensity of seismic activity markedly decrease. It was concluded that the frequency and intensity of seismic special are the cause of the positive IGA values that are found in the LMS. The active faulting both cause earthquakes and result in the localized crustal uplift that causes the observed IGA.

(2) In the LMS orogenic belt, the dominant focal depth of strong earthquakes has historically been 13–20 km. For

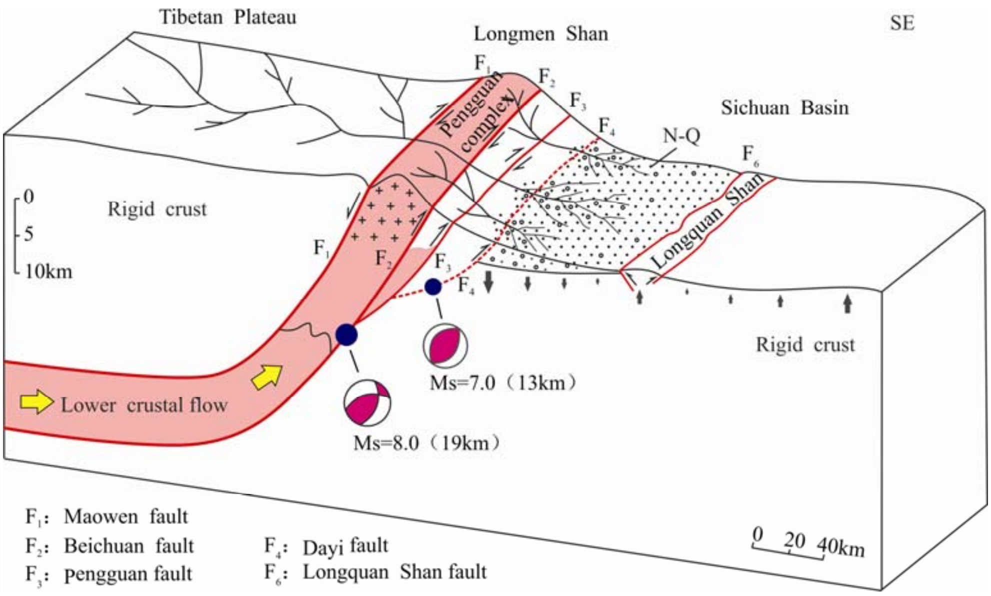

Fig. 14. Dynamic model of the relationship between surface processes and lower crustal flow on the eastern margin of the Tibetan Plateau.

example, the focal depths of the Wenchuan and Lushan Earthquakes were 19 km and 13 km respectively. The dominant focal depth coincides with the depth of the lower crustal flow, from which it may be inferred that the strong earthquakes originate in the lower crustal flow. The direction of the principal stress in the earthquakes is generally northwesterly, which is perpendicular to the LMS orogenic belt.

(3) The Wenchuan Earthquake was characterized as a thrust-dextral strike-slip earthquake (Xu et al., 2009; Densmore et al., 2010; Li et al., 2011). The Pengguan and Beichuan Faults, which are parallel thrust faults, are both located in the belt of abrupt IGA changes. As a result, limited (i.e., localized) tectonic shortening and a narrow belt of tectonic loading are produced in the LMS. We therefore suggest that the atypical parallel surface rupture zones from the Wenchuan Earthquake were induced by lower crustal flow in the LMS as well as by local shortening (Fig. 14).

6.3 Time of formation of the positive IGA and lower crustal flow in LMS

Royden et al. (1997) suggested that lower crustal flow reached the eastern edge of the Tibetan Plateau at approximately 15–10 Ma. Burchfiel et al. (2008) suggested that the modern high topography and lower crustal flow in the LMS might have been formed at 12–5 Ma; Kirby et al. (2003, 2008) suggested 15–8 Ma. Simon et al. (2003), on the basis of shortening and surface deformations, proposed that lower crustal flow might have commenced in the LMS around 4 Ma. The Precambrian Pengguan and Baoxing Complexes are important components of the LMS and have been representative elements of these mountains since the Cenozoic. There were also important differences in the LMS in the Cenozoic and in the Mesozoic. Low-temperature thermochronological data indicates that three cooling events have taken place in the Pengguan and Baoxing Complexes since the Cenozoic, at 30–25 Ma (Wang et al., 2012), at 10–4 Ma (Liu Shugen, 1993) and at 5–1.7 Ma (Tan Xibin al., 2013). When and how these complexes were uplifted and unroofed at the surface is still an important problem in the evolutionary history of the LMS.

In the present work, we concluded from correlating the high-density Precambrian Pengguan and Baoxing complexes with the positive IGA values that the two are obviously related. They have the same formation mechanisms and periods. Consequently, the outcrops of the complexes provide evidence that uplift was due to the upheaving action of lower crustal flow. Therefore, we suggest that establishing the time when the Precambrian complexes were unroofed at the surface could be used to calibrate the formation time of the positive IGA values and lower crustal flow in the LMS. The first gravels from weathering of the complexes appear in the Dayi Conglomerate layer in the Chengdu Basin have been dated to 3.6 Ma (Li Yong et al., 1995). We therefore suggest that the lower crustal flow in the LMS formed at 3.6 Ma or slightly earlier, which approximates closely to the 4 Ma date proposed by Simon et al. (2003). This would have resulted in the extremely high positive IGA values, the tectonic load and the high topography of the LMS.

7 Conclusions

This study investigated the dynamic relationship between the positive IGA values and the lower crustal flow in the LMS since 3.6Ma. The main conclusions are listed below.

(1) The IGA map on the eastern margin of the Tibetan Plateau was plotted, and the data was found to be divided into a weakly negative zone on the Tibetan Plateau, a positive zone in the LMS, and a negative zone in the Sichuan Basin.

(2) By correlating the IGA map with a digital elevation map, a topographic relief map, a tectonic map and a rock density map, we propose that the zones of abrupt changes in IGA values correspond to abrupt changes of topography, crustal thickness, rock density and the seismogenic belt in the LMS.

(3) Based on the Airy isostasy model, the positive IGA values were simulated by calculating the gravity anomalies in quasi-3D bodies. The results suggest that the high-angle front and rear faults of the LMS dip towards the northwest, without a mountain root. The top of the lower crust was uplifted by approximately 11 km, which is responsible for the positive IGA values, the tectonic load and the density load in the LMS. We also propose that the heaving uplift force of a lower crustal flow propelled the dynamic uplift mechanisms in the LMS.

(4) Elastic flexure simulations were conducted along the lines of the Watts flexural isostasy model by calculating the tectonic load in the LMS and the asymmetrical flexural subsidence in the foreland basin (i.e., the Western Sichuan Basin). The results suggested that limited tectonic shortening in the LMS, a narrow tectonic load and a density load driven by lower crustal flow led to asymmetrical flexural subsidence in the foreland basin and uplift on the forebulge.

(5) The correspondence between zones of extremely high positive IGA values and the Precambrian Pengguan–Baoxing Complexes in the LMS is significant. Gravels from weathering of the unroofed Precambrian complexes first appeared in the Dayi conglomerate layer in Chengdu

Basin, evidence that the lower crustal flow beneath the LMS, and the positive IGA values that reflect this, were formed around 3.6 Ma or slightly earlier.

Acknowledgements

We thank the Geophysical Prospecting Team of Sichuan Bureau of Geology and Mineral Resources (GPTSBGMR) for providing the raw gravity data. We appreciate profess Jiashun Yu from Geological and Nuclear Sciences, New Zealand, who provide a lot of assistance during modifying the manuscript. This study was funded by the National Natural Science Foundation of China (Grant Nos. 41372114, 41502116, 41340005, 41172162, 40972083, 40841010), and a research project of the National Key Laboratory of Oil and Gas Reservoir Geology and Exploitation (Grant No. SK-0801).

Manuscript received July. 18, 2016
accepted Aug. 10, 2016
edited by Liu Lian

References

Burchfiel, B.C., Chen, Z., and Liu, Y., 1995. Tectonics of the Longmen Shan and adjacent regions, central China. *International Geological Review*, 37(8): 661–735.

Burchfiel, B.C., Royden, L.H., vander, R.D., and Hager, B.H., 2008. A geological and geophysical context for the Wenchuan earthquake of 12 May 2008, Sichuan, People's Republic of China. *GSA Today*, 18(7) : 4–11

Bird, P, 1991. Lateral extrusion of lower crust from under high topography in the isostatic limit. *Journal of Geophysical Research*, 96(B6): 10275–10286.

Burov, E., and Diament, M., 1996. Isostasy, equivalent elastic thickness, and inelastic rheology of continents and oceans. *Geology*, 24: 419–422.

Clark, M.K., and Royden, L.H., 2000. Topographic ooze: building the eastern margin of Tibet by lower crustal flow. *Geology*, 28: 703–706.

Chen, Z., Burchfiel, B.C., Lin, Y., King, R.W., Royden, L.H., Tang, W., Wang, E., Zhao, J., and Zhang, X., 2001. Global positioning system measurements from eastern Tibet and their implications for India/Eurasia intercontinental deformation. *Journal of Geophysical Research*, 105(B7): 16215–16227.

de Michele M., Raucoules, D., de Sigoyer J., Pubellier, M., and Chamot, R.N., 2010. Three-dimensional surface displacement of the 2008 May 12 Sichuan earthquake (China) derived from Synthetic Aperture Radar: evidence for rupture on a blind thrust. *Geophysical Journal International*, 183(3): 1097–1103.

Densmore, A.L., Li, Y., Ellis, M.A., and Zhou, R., 2005. Active tectonics and erosional unloading at the eastern margin of the Qinghai-Tibet Plateau. *Journal of Mountain Science*, 2(2): 146 –154.

Densmore, A.L., Ellis, M.A., Li, Y., Zhou, R., Hancock, G.S., and Richardson, N.J., 2007. Active tectonics of the Beichuan and Pengguan faults at the eastern margin of the Qinghai-Tibet Plateau. *Tectonics*，80(8): 113–127.

Densmore, A.L., Li, Y., Richardson, N.J., Zhou, R., and Zhang, Y., 2010. The role of late Quaternary upper-crustal faults in the 12 May 2008 Wenchuan Earthquake. *Bulletin of the Seismological Society of America*, 100(5B): 2700–2712. DOI: 10. 1785/0120090294.

England, P., and Molnar, P., 1990. Surface uplift, uplift of rocks,and exhumation of rocks. *Geology*, 18(12): p.1173–1177.

Enkelmann, E., Ratschbacher, L., Jonckheere, R., Nestler, R., Fleischer, M., Gloaguen, R., Hacker, B.R., Zhang, Y., and Ma Y.S., 2006. Cenozoic exhumation and deformation of northeastern Tibet and the Qinling: Is Tibetan lower crustal flow diverging around the Sichuan Basin? *GSA Bulletin*, 118 (5/6): 651–671.

Fu, B., Shi, P., Guo, H., Okuyama, S., Ninomiya, Y., and Wright, S., 2011. Surface deformation related to the 2008 Wenchuan earthquake, and mountain building of the Longmen Shan, eastern Qinghai-Tibet Plateau. *Journal of Asian Earth Sciences*, 40: 805–824.

Fu, G., Gao, S., Freymueller, J.T., Zhang, G., Zhu, Y., and Yang, G., 2014. Bouguer gravity anomaly and isostasy at western Sichuan Basin revealed by new gravity surveys. *Journal of Geophysical Research: Solid Earth*, 119: 3925–3938.

GPTSBGMR (Geophysical Prospecting Team of Sichuan Bureau of Geology and Mineral Resources), 1991. *The comprehensive research report of gravity anomalies and aeromagnetic anomalies in Sichuan province*.

Hubbard, J., and Shaw, J.H., 2009. Uplift of the Longmen Shan and Qinghai-Tibet Plateau, and the 2008 Wenchuan (M=7.9) earthquake. *Nature*, 458: 194–197.

Hu Yuanxin, Liu Xinrong, Xu Hui and Ge Hua, 2010. Multiple linear regression models to predict the uniaxial compressive strength and the elastic modulus of Pengguan complex. *Geotechnical Investigation & Surveying*, 12: 15–21(in Chinese with English Abstract).

Hetenyi, R., 1974. *Beams on elastic foundation: Ann Arbor*. Michigan: University of Michigan Press, 255.

Jordan, T.A., and Watts, A.B., 2005. Gravity anomalies, flexure and the elastic thickness structure of the India–Eurasia collisional system. *Earth and Planetary Science Letters*, 236 : 732–750

Kirby, E., and Whipple, K., 2003. Distribution of active rock uplift along the eastern margin of the Tibetan Plateau: Inferences from bedrock channel longitudinal profiles. *Journal of Geophysical Research*, 108(B4): 2217.

Kirby, E., Whipple, K., and Harkins, N., 2008. Topography reveals seismic hazard. *Nature Geoscience*, 1: 485–487.

Li, Y., Zhou, R., and Densmore, A.L., 2006. *The Geology of the Eastern Margin of the Qinghai-Tiben Plateau*. Beijing: Geological Publishing House, 168.

Li Yong, Zeng Yunfu and Yi Haisheng, 1995. *Sedimentary and Tectonic Evolution of Longmengshan foreland basin, western Sichuan China*. Press of Chengdu University of Science and Technology, Chengdu, 153 (in Chinese with English Abstract).

Li, Y., Allen, P.A., Densmore, A.L., and Xu, Q., 2003. Evolution of the Longmen Shan foreland basin (western Sichuan, China) during the Late Triassic Indosinian Orogeny. *Basin Research*, 15: 117–138.

Li Yong, Xu Gongda, Zhou Rongjun, Densmore A. L. and Ellis M. A., 2005. Isostatic gravity anomalies in the Longmen mountains and their constraints on the crustal uplift below the mountains on the eastern margin of Qinghai-Tibet Plateau.

Geological Bulletin of China, 24(12): 1162–1169 (in Chinese with English Abstract).

Li, Y., Zhou, R., Densmore, A.L., Cao, S., and Liu, Y., 2011. Spatial relationships between surface ruptures in the Ms 8. 0 Earthquake, the Longmen Shan region, Sichuan, China. *Journal of Earthquake and Tsunami*, 5(4): 329–342.

Li Yong, Yan Liang, Shao Chongjian, Wang Zhengjiang, Yan Zhaokun, Yu Qian, Zhou Rongjun and Li Haibing, 2017. The Coupling Relationship between the Uplift of Longmen Shan and the Subsidence of Foreland Basin, Sichuan, China. *Acta Geologica Sinica* (English Edition), 91(2): 379–395.

Liu Shugen, 1993. *The Formation and Evolution of Longmengshan thrust zone and western Sichuan foreland basin, China*. Chengdu: Press of Chengdu University of Science and Technology,167 (in Chinese with English Abstract).

Liu Beili, 1994. Analysis and application of density data of rocks from Sichuan province. *Geophysical and Geochemical Exploration*, 18(3): 232–237 (in Chinese with English Abstract).

Meng, Q., Hu, J., Wang, E., and Qu, H., 2006. Late Cenozoic denudation by large-magnitude landslides in the eastern edge of Qinghai-Tibet Plateau. *Earth and Planetary Science Letters*, 243(1–2): 252–267.

Molnar, P., 2012. Isostasy can't be ignored. *Nature Geoscience*, 5: 83–83.

Parker, R.N., Densmore, A.L., Rosser, N.J., Michele, M.D., Li, Y., Huang, R., Whadcoat, S., and Petley, D.N., 2011. Mass wasting triggered by the 2008 Wenchuan earthquake is greater than orogenic growth. *Nature Geoscience*, 4: 449–452.

Qiu Jun, Wu Manlu, Fan Taoyuan, Zhang Chong, Li Ran and Chen Lizhong, 2017. Comparative Analysis of In situ Stress State in the Southwestern Segment of Longmenshan Fault Zone before and after Lushan Earthquake. *Acta Geologica Sinica*, 91(5): 969–978 (in Chinese with English Abstract).

Royden, L.H., Burchfiel, B.C., King, R.W., Wang, E., Chen, Z., Shen, F., and Liu, Y., 1997. Surface deformation and lower crustal flow in eastern Tibet. *Science*, 276, 788 – 790.

Richardson, N.J., Densmore, A.L., Seward, D., Fowler, A., Wipf, M., Li, Y., Ellis, M.A. and Zhang, Y., 2008. Extraordinary denudation in the Sichuan Basin: insights from low-temperature thermochronology adjacent to the eastern margin of the Qinghai-Tibet Plateau. *Journal of Geophysical Research*, 113, B04409, doi:10.1029/2006JB004739.

Simon, W., Tatsuki, T., Mutsuki, A., Tetsuo, K., Kentaro, T., Kazuhiro, S., and Hironobu, H., 2003. Cenozoic and Mesozoic metamorphism in the Longmenshan orogeny: implications for geodynamic models of eastern Tibet. *Geology*, 31(9): 745–748.

Stewart, J., and Watts, A.B., 1997. Gravity anomalies and spatial variations of flexural rigidity at mountain ranges. *Journal of Geophysical Research*, 102(B3): 5327–5352.

Tan Xibin, Xu Xiwei, Lee Yuanhsi, Kang Wenjun and Zhao Shiliang, 2016. Cenozoic Denudation and Vertical Faulting History of the Central Segment of the Longmenshan Thrust Bel. *Acta Geologica Sinica* (English Edition), 90(4): 1541–1542.

Tan Xibin, Li Yuanxi, Xu Xiwei, Chen Wenyu, Xu Chong and Yu Guihua, 2013. Cenozoic fault activity of the southern segment of the Longmenshan thrust belt: evidence from low-temperature thermochronology data. *Seismology and Geology*, 35(3): 506–517 (in Chinese with English Abstract).

Watts, A.B., 1992. The effective elastic thickness of the lithosphere and the evolution of foreland basins. *Basin Research*, 4: 169–178.

Watts, A.B., 2001. *Isostasy and Flexure of the Lithosphere*. Cambridge. New York, Melbourne: Cambridge University Press, 480.

Wang, E, Kirby, E., Furlong, K.P., van Soest, M., Xu, G., Shi, X., Kamp, P.J.J., and Hodges, K.V., 2012. Two-phase growth of high topography in eastern Tibet during the Cenozoic. *Nature Geoscience*, 5(9): 640–645.

Wang Qianshen, Teng Jiwen, Zhang Yongqian and Yang Hui, 2008. The effect of crustal gravity isostasy and Wenchuan earthquake in Longmenshan faults and adjacent area. *Progress in Geophysics*, 23(6): 1664–1670 (in Chinese with English Abstract).

Xu, X., Wen, X., Yu, G., Chen, G., Klinger, Y., Hubbard, J., and Shaw, J., 2009. Coseismic reverse-and oblique-slip surface faulting generated by the 2008 Mw7. 9 Wenchuan earthquake, China. *Geology*, 37(6): 515–518.

Xu, G., and Kamp, P.J.J., 2000. Tectonics and denudation adjacent to the Xianshuihe fault, eastern Qinghai-Tibet Plateau: Constraints from fission track thermochronology. *Journal of Geophysical Research*, 105(B8): 19231–19251.

Xu Zhiqin, Hou Liwei and Wang Zongxiu, 1992. *Orogenic Processes of the Songpan- Garze Orogenic Belt of China*. Beijing: Geology Publish House, 199.

Xu Zhiqin, Li Huaqi, Hou Liwei, Fu Xiaofang, Chen Wen, Zeng Lingsen, Cai Zhihui and Chen Fangyuan, 2007. Uplift of the Longmen-Jinping orogenic belt along the eastern margin of the Qinghai-Tibet Plateau: Large-scale detachment faulting and extrusion mechanism. *Geological Bulletin of China*, 26 (10): 1262–1276 (in Chinese with English Abstract).

Yan Zhaokun, Li Yong, Shao Chongjian, Zhou Rongjun, Yan Liang, Zhao Guohua and Yan Binglei, 2016. Interpreting the Coseismic Uplift and Subsidence of the Longmen Shan Foreland Basin System during the Wenchuan Earthquake by a Elastic Flexural Model. *Acta Geologica Sinica* (English Edition), 90(2): 555–566.

Yan Zhaokun, Wang Xuben, Li Yong, Luo Wei, Yang Yihai, Wang Xingjian, Shao Chongjian and Yan Liang, 2017. Coupling between the dynamic processes at depth and geologic processes on the surface of the Longmenshan thrust belt. *Chinese Journal of Geophysics*, 60(7): 2744–2755 (in Chinese with English Abstract).

Zhang, P., Shen, Z., Wang, M., Gan, W., Bürgmann, R., Molnar, P., Wang, Q., Niu, Z., Sun, J., Wu, J., Sun, H., and You X., 2004. Continuous deformation of the Qinghai-Tibet Plateau from global positioning system data. *Geology*, 32: 809–812.

About the first author

LI Yong, male; born in 1963 in Nanjing City, Jiangsu Province; PhD; graduated from Chengdu university of technology; professor of Chengdu university of technology. He is now interested in the study on orogenic belt and sedimentary basin, active tectonics and process of the earth's surface. Email: liy@cdut.edu.cn; phone: 028–84079759.